Hindawi
Shock and Vibration
Volume 2019, Article ID 7275425, 11 pages
https://doi.org/10.1155/2019/7275425

Research Article

Theoretical and Experimental Study on Damage Properties of Surrounding Rock under High-Frequency Constant Impact Load

Zhi Liu,[1] **Wanrong Wu**,[1] **Zhuang Yao**,[1] **and Qianhua Hao**[1,2]

[1]*College of Mechanical and Electrical Engineering, Central South University, Changsha 410083, China*
[2]*School of Energy and Electromechanical, Hunan University of Humanities, Science and Technology, Loudi 417000, China*

Correspondence should be addressed to Wanrong Wu; wwr@csu.edu.cn

Received 25 February 2019; Accepted 8 April 2019; Published 12 May 2019

Academic Editor: Chengzhi Shi

This paper aims to investigate the mechanics and damage properties of granite by drilling a center hole in Φ50 × 100 mm standard granite specimens under high-frequency constant impact load and then applying them to the uniaxial compression experiment through the INSTRON 1346 universal material testing machine. According to the experimental results, under constant impact load, as the center hole diameter increases, the peak stress of the rock specimen increases accordingly and the effective elastic modulus of the rock specimen decreases first and then increases gradually. In this study, by theoretical analysis of the surrounding rock damage caused under high-frequency impact load, a statistical damage constitutive model that has taken surrounding rock damage into consideration is established on the basis of the Weibull distribution. Meanwhile, the experimental curve is obtained to analyze the damage and damage radius of surrounding rock under high-frequency impact load. The results show that the surrounding rock damage and damage ratio (the ratio of damage radius to center hole radius) of rock decrease with the increase of the center hole diameter. This model that can effectively describe the damage laws of surrounding rock under impact load serves as a guide for the design and development of composite rock-drilling tools.

1. Introduction

With the development of open-pit mining at home and abroad in the trend towards high efficiency, energy conservation, and environmental protection, conventional drilling methods such as rock impact, crushing, and cutting make it difficult to achieve further enlargement of the hole diameter, improvement of rock-drilling efficiency, and reduction of energy consumption. Many problems such as tunneling, mining, and river dredging in geotechnical engineering involve how to accelerate rock damage to improve drilling efficiency and reduce energy consumption, which have promoted the rapid development of rock damage mechanics and rock fracture mechanics and gradually become hot research directions in the field of rock mechanics [1]. Tunneling and mining often adopt the rock-breaking method of drilling and blasting that is mainly characterized by its use of high strain rate impact load to cause rock fracture or damage. A number of domestic and international experts have explored the rock constitutive model and mechanics properties under impact load in the perspective of strain rate [2–7] and improved SHPB (split Hopkinson pressure bar) apparatus to study the mechanics, damage properties, uniaxial compressive strength, elastic modulus, and the law of energy absorption of standard rock specimens and rock specimens containing preexisting cracks under different impact loads that are obtained by putting different pressures on the hammer of the SHPB apparatus. The dynamic failure process of rock specimens with a center hole under dynamic load coupled with static load is further studied by the use of high-speed camera [8–15].

Drilling and blasting usually take place many times in the excavation of engineering rock mass and tunneling;

therefore, the surrounding rock around the hole undergoes repeated impact loads [16–18]. Some scholars have argued that wave impedance, wave velocity, and so on can be applied to describe the degree of rock damage under cyclic impact load. They have also analyzed the influences of surrounding rock stress, impact load, and impact frequency on damage and studied how situ stress, tunnel shape, and excavation method affect the development of the excavation damage zone (EDZ) [19–23].

In order to study the damage problems of surrounding rocks induced by tunnel excavation and explore the rock damage evolution laws under dynamic load coupled with static load, some new techniques and methods have been applied such as ultrasonic computed tomography, nuclear magnetic resonance technique, acoustic emission technique, and ultrasonic testing method [24–26]. The influences of stress redistribution on surrounding rock damage during the blasting excavation of deep tunnels and the impacts of the homogeneous index and confining pressure on the tunnel failure mode are investigated with the aid of 3D numerical simulation software. Numerical simulations can further be used to analyze not only the extension of crack length of rock specimens with preexisting cracks and a center hole but also the variation relation of damage area with time [27–30]. Experts like Wang Zhengyi have set up a damage model of roadway surrounding rock on the basis of Mohr–Coulomb's strength theory and investigated the properties of surrounding rock damage and dynamic response under oblique incidence dynamic load [31].

In this study, the compound rock-drilling principle (a center hole is drilled first through the impactor on a standard rock specimen, causing damage to its surrounding rock, and then the reaming cone is used to ream holes on the damage area), shown in Figure 1, is applied to drilling rock specimens under high frequency through the electric hammer impact in a case study of granite. By theoretical analysis of the surrounding rock damage under high-frequency impact load, a statistical damage constitutive model that has taken surrounding rock damage into consideration is established on the basis of the Weibull distribution. This paper combines theoretical research with experimental results, aiming to explore the damage evolution laws of rock specimens and the damage radius of surrounding rock under high-frequency impact load, thus serving as a scientific guide for the structure design of the compound rock-drilling machine in Figure 1.

2. Study of Rock Damage Area under Impact Load

2.1. Analysis of Rock Stress under Impact Load. The stress state of rock specimens under the impact of drill bit can be approximately considered the Boussinesq problem. Under impact load, take one unit on the border of the semi-infinite elastic body as an example for stress analysis, which is illustrated in Figure 2.

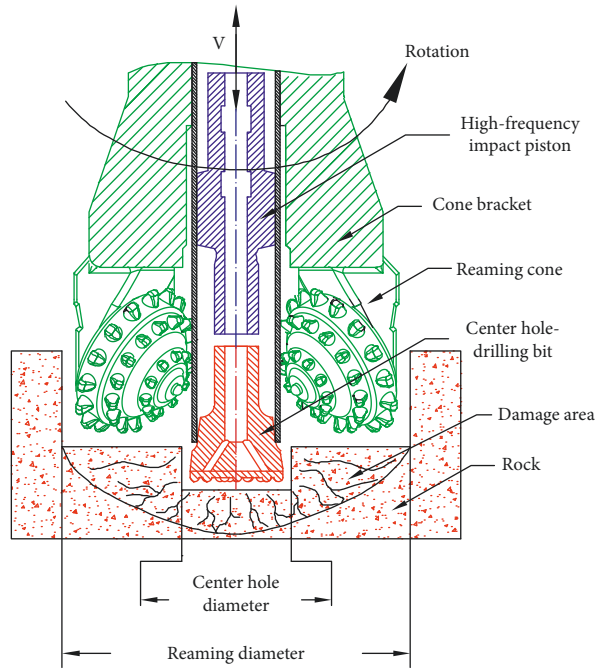

Figure 1: Schematic diagram of compound rock drilling.

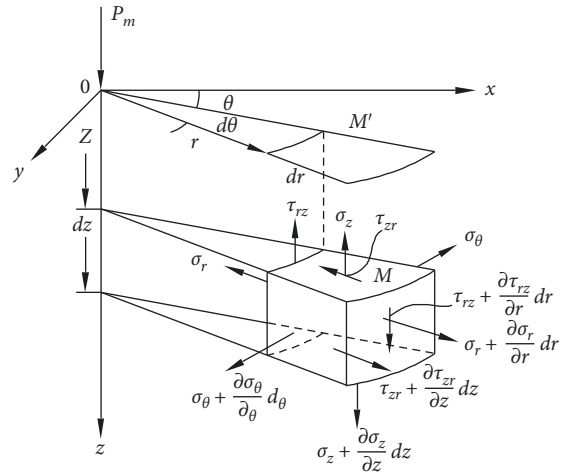

Figure 2: Stress analysis of the element.

Each stress component is expressed as follows:

$$\begin{cases} \sigma_r = \dfrac{P_m}{2\pi}\left\{(1-2\mu)\left[\dfrac{1}{r^2} - \dfrac{Z}{r^2}\left(r^2+Z^2\right)^{-1/2}\right] - 3r^2 Z\left(r^2+Z^2\right)^{-5/2}\right\}, \\ \sigma_\theta = \dfrac{P_m}{2\pi}(1-2\mu)\left[-\dfrac{1}{r^2} + \dfrac{Z}{r^2}\left(r^2+Z^2\right)^{-1/2} + Z\left(r^2+Z^2\right)^{-3/2}\right], \\ \sigma_Z = -\dfrac{3}{2}\dfrac{P_m}{\pi} Z^3\left(r^2+Z^2\right)^{-5/2}, \\ \tau_{rz} = \tau_{zr} = -\dfrac{3}{2}\dfrac{P_m}{\pi} rZ\left(r^2+Z^2\right)^{-5/2}, \end{cases} \quad (1)$$

where σ_r, σ_θ, and σ_z denote the radial normal stress, the circumferential normal stress, and the axial normal stress, respectively; P_m denotes the impact load; μ denotes Poisson's ratio; and τ_{rz} and τ_{zr} stand for the axial shear stress and the radial shear stress.

2.2. Distribution of Elastic and Plastic Zones. After a center hole is drilled, the elastic and plastic zone distribution of the surrounding rock can be illustrated in Figure 3; that is, the range of the plastic zone is $a < r \le r_1$, the range of the elastic zone is $r_1 < r \le r_2$, and the range of the original rock zone is $r_2 < r$.

According to Figures 2 and 3, since $Z = 0$ in the process of drilling operations, the radial plastic stress σ_r of the center hole wall ($L = a$) under the impact load P_m turns out to be

$$\sigma_r = \frac{1-2\mu}{r^2} \cdot \frac{P_m}{2\pi}. \tag{2}$$

According to Mohr–Coulomb's strength theory, the ultimate stress circle can be expressed as

$$\frac{\sigma_r - \sigma_\theta}{2} = \left[\frac{\sigma_\theta - \sigma_r}{2} + \sigma_r + c \cdot \cot\phi\right] \cdot \sin\phi. \tag{3}$$

In order to define the plastic zone radius r_1, the elastic zone can be considered a thick-walled cylinder with the internal diameter of r_1. Suppose the original rock stress is σ_0 and the radial normal stress of the border between elastic zone and plastic zone is σ_{r1}, the radial normal stress σ_{re} and circumferential normal stress $\sigma_{\theta e}$ at any point in the thick-walled cylinder or the plastic zone can be calculated on the basis of mechanics of materials as follows:

$$\begin{cases} \sigma_{re} = \sigma_0 + (\sigma_{r1} - \sigma_0)\dfrac{r_1^2}{r^2}, \\ \sigma_{\theta e} = \sigma_0 + (\sigma_0 - \sigma_{r1})\dfrac{r_1^2}{r^2}. \end{cases} \tag{4}$$

Adding together the above two expressions in formula (4), we get

$$(\sigma_{re} + \sigma_{\theta e}) = 2\sigma_0. \tag{5}$$

On the border between elastic zone and plastic zone where $\sigma_r = \sigma_{re}$, $\sigma_\theta = \sigma_{\theta e}$; substituting $r = r_1$ in formula (2), according to formulas (3) and (5), the radial normal stress in the plastic zone σ_r and circumferential normal stress in the plastic zone σ_θ on the border between elastic zone and plastic zone can be expressed as

$$\begin{cases} \sigma_r = \sigma_0(1 + \sin\phi) + c \cdot \cos\phi, \\ \sigma_\theta = \sigma_0(1 - \sin\phi) - c \cdot \cos\phi. \end{cases} \tag{6}$$

Based on formulas (2) and (6), the plastic zone radius can be expressed as

$$r_1 = \left(\frac{P_m(1-2\mu)}{2\pi \cdot (\sigma_0(1+\sin\phi) + c \cdot \cos\phi)}\right)^{1/2}. \tag{7}$$

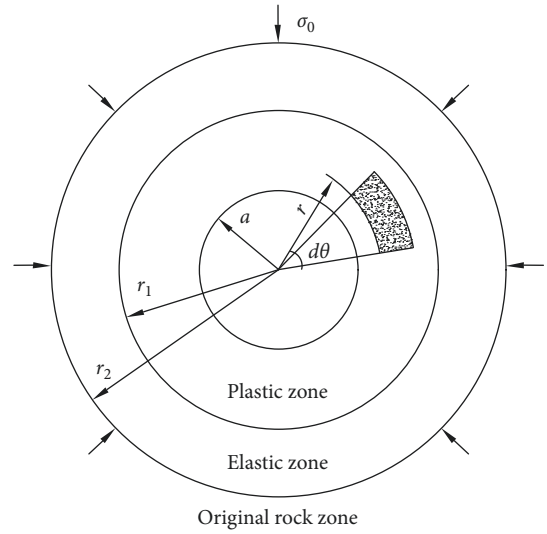

Figure 3: Elastic and plastic zone distribution of the surrounding rock.

According to the plastic zone radius, the surrounding rock damage can be defined as

$$D_0 = \frac{\pi(r_1^2 - a^2)}{\pi(R^2 - a^2)}, \tag{8}$$

where R stands for the external diameter of the rock specimen.

3. The Rock Constitutive Equation under High-Frequency Impact Load

3.1. Basic Assumption. A rock unit can be regarded as a parallel combination of damage mass and viscous body. As the surrounding rock damage D_0 is caused under high-frequency impact load, the mechanical model of the rock element, shown in Figure 4, can be considered a series connection of the mentioned parallel combination and surrounding rock damage D_0. The following are three assumptions.

(1) The viscous body has no damage property and does not work under approximate static load at a relatively low loading rate. The viscous body abides by the following constitutive relation:

$$\sigma_b = \eta \frac{d\varepsilon}{dt}, \tag{9}$$

where σ_b is the stress of the viscous body, ε the strain of the viscous body, t the time, and η the viscosity coefficient that reflects the viscosity property of rock and can be measured by the creep experiment of rock. The viscosity coefficient of rock generally ranges from 0.1 to 0.5.

(2) The strength of damage mass of every element complies with the laws of the Weibull distribution, and its probability density function is

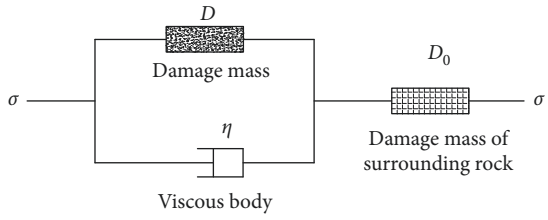

Figure 4: Mechanical model of the rock element.

$$p(F) = \frac{m}{F_0}\left(\frac{F}{F_0}\right)^{m-1} \exp\left[-\left(\frac{F}{F_0}\right)^m\right], \tag{10}$$

where F denotes the random distribution variable of element strength, m the shape parameter of the Weibull distribution, and F_0 the scale parameter of the Weibull distribution.

(3) The damage mass is macroscopically isotropic. It possesses a property of linear elasticity before damage and loses its carrying capacity after damage.

3.2. Statistical Damage Variable. Assuming that constant damages to elements give rise to the fracture of rock specimens, the original number of elements of the rock specimen is N, and the number of ruptured elements under certain load F is N_f, the statistical damage variable D can be defined as

$$D = \frac{N_f}{N}. \tag{11}$$

Based on formula (11), N_f can be deduced:

$$N_f = \int_0^F N p(y) dy. \tag{12}$$

By considering formulas (8), (11), and (12), the statistical damage variable D is deduced based on the Weibull distribution:

$$D = 1 - \exp\left[-\left(\frac{F}{F_0}\right)^m\right]. \tag{13}$$

According to formula (13), the damage variable has something to do with the strength of the rock element influenced by the stress state. In order to show the impact of a complicated stress state on the rock strength in consideration of the failure criterion of rocks, assume the general failure criterion of the rock element is

$$f(\sigma_0) - k_0 = 0, \tag{14}$$

where $f(\sigma_0)$ stands for the function associated with the stress state and k_0 is the material constant.

The Drucker–Prager failure criterion is characterized by certain advantages such as simple parameter forms and extensive applications in rock materials. On the basis of the Drucker–Prager failure criterion, the strength of the rock element can be set as

$$F = f(\sigma) = \alpha I_1 + \sqrt{J_2}, \tag{15}$$

$$\alpha = \frac{\sin\phi}{\sqrt{9 + 3\sin^2\phi}}, \tag{16}$$

where ϕ denotes the angle of internal friction, I_1 the first invariant of stress tensor, and J_2 the second invariant of stress deviator. According to Hooke's law,

$$I_1 = \frac{(\sigma_1 + 2\sigma_3)E\varepsilon_1}{\sigma_1 - 2\mu\sigma_3}, \tag{17}$$

$$\sqrt{J_2} = \frac{(\sigma_1 - \sigma_3)E\varepsilon_1}{\sqrt{3}(\sigma_1 - 2\mu\sigma_3)}, \tag{18}$$

where σ_1 denotes the maximum principal stress, σ_3 the minimum principal stress, ε the strain, and E Young's modulus of elasticity.

Under no confining pressure, that is, in the one-dimensional stress state, the minimum principal stress $\sigma_3 = 0$ and the strain $\varepsilon_1 = \varepsilon$. By considering formulas (15)–(18), it can be deduced that

$$F = \left(\alpha + \frac{1}{\sqrt{3}}\right)E\varepsilon. \tag{19}$$

3.3. The Constitutive Model of Rock. As the element model is a parallel combination, its strain equals that of the two divided units in total, and so does its stress. The rock specimen has undergone certain damage D_0 after being drilled the center hole under high-frequency impact load; therefore, on the basis of the strain equivalence hypothesis, the constitutive equation of rock under high-frequency impact load can be expressed as follows:

$$\sigma = E\varepsilon(1 - D - D_0) = E\varepsilon\left\{\exp\left[-\left(\frac{F}{F_0}\right)^m\right] - D_0\right\} + \eta\frac{d\varepsilon}{dt}. \tag{20}$$

As the uniaxial compression experiment is conducted under approximate static load at a relatively low loading rate, the constitutive relation of rock under high-frequency impact load can be expressed without considering the stress of the viscous body as follows:

$$\sigma = E\varepsilon(1 - D - D_0) = E\varepsilon\left\{\exp\left[-\left(\frac{F}{F_0}\right)^m\right] - D_0\right\}. \tag{21}$$

3.4. Calculation of Model Parameters. According to the constitutive relation of the damage model, the key to set up a constitutive model is to define the model parameters m and F_0. Based on the extremum problem of multivariate function, the slope of the vertex of the stress-strain curve is zero; that is, the coordinate of the peak point of the stress-strain curve is $(\sigma_m, \varepsilon_m)$, which can be mathematically expressed as

$$\frac{d\sigma}{d\varepsilon}\Big|(\sigma_m, \varepsilon_m) = 0, \tag{22}$$

where σ_m and ε_m stand for peak stress and peak strain, respectively.

Plugging the peak value into formula (21) and combining it with formula (22), the damage model parameters m and F_0 can be expressed as follows:

$$m = \left(1 - \frac{D_0}{\exp\left(-\ln\left(\left(\sigma_m/E\varepsilon_m\right) + D_0\right)\right)}\right) \cdot \frac{1}{\ln\left(\left(\sigma_m/E\varepsilon_m\right) + D_0\right)},$$

$$F_0 = \frac{\left(\alpha + \frac{1}{\sqrt{3}}\right)E\varepsilon_m}{\left(-\ln\left(\left(\sigma_m/E\varepsilon_m\right) + D_0\right)\right)^{1/m}}. \tag{23}$$

4. Experimental Verification

4.1. Preparation of Rock Specimens. Granite is selected as the test rock specimen for its integral and dense structure, solid texture, and no obvious macroscopic cracks on its surface. The dimension of the test specimen under static load is $\Phi 50 \times 100$ mm that meets the experimental performance-testing requirements of rock mechanics. The flatness and parallelism at both head faces of the specimen are less than 0.02 mm. As is illustrated in Figure 5, the rock specimens in Figure 6 are processed by applying the electric hammer to drilling the center hole. The MTS 815 rock mechanics testing system from the Institute of Mechanics Properties in the Advanced Research Center of Central South University is first used to determine the physical and mechanical parameters of granite that are shown in Table 1.

4.2. Experimental Equipment and Principle. The rock specimens pasted with strain gauges are applied to carry out uniaxial compression experiments by the INSTRON 1346 universal material testing machine from the Institute of Mechanics Properties in the Advanced Research Center of Central South University. The maximum load range of the testing machine is 2000 kN for static load and 1000 kN for dynamic load. Its measurement accuracy is ±0.5%. Through these uniaxial compression experiments, the stress-strain curve, Poisson's ratio, and elastic modulus of every rock specimen can be obtained. Figure 7 shows two photos taken in the experimental process.

4.3. Experimental Approach. In order to explore the damage properties and dimension of the damage area of granite under high-frequency impact load, 5 standard rock specimens are chosen as a contrast group and 15 others that are drilled the center hole by an electric hammer are divided into three experimental groups with different center hole diameters, Φ6 mm, Φ8 mm, and Φ10 mm, respectively. The INSTRON 1346 universal material testing machine has done uniaxial compression experiments on the 20 rock specimens to determine the stress-strain curve of every rock specimen. The physical parameters of granite specimens are listed in Table 2.

4.4. Experimental Results. By processing the experimental data of 20 rock specimens in four groups, four data from each specimen group are selected, and the stress-strain curves of the selected rock specimens can be drawn. As is illustrated in Figure 8, the peak stress of every rock specimen is marked in the stress-strain curves of the four groups.

By the analysis of the stress-strain curves of specimen groups in Figure 8, the initial stage of the stress-strain curve of all the specimens almost coincides before they fail; in other words, the initial elastic modulus of every rock specimen is almost the same. With the increase of load force, the slope of the ascending curve gradually increases, which indicates that the initial crack inside the rock has closed, causing the increase of elastic modulus. Before the arrival of peak stress, the slope of the stress-strain curve gradually decreases, demonstrating the expansion of initial cracks as the rock specimen gains energy with the increase of load force, which leads to the decrease of the elastic modulus and deterioration of the properties of materials [32].

Judging from the peak stress of every rock specimen in the stress-strain curve, the peak stress of the standard rock specimen with a center hole is lower than that of the rock specimen with no center hole. Besides, among the three groups of rock specimens with different center hole diameters, the specimen group with the center hole diameter of Φ6 mm has the lowest average peak stress of 140.59 MPa, the specimen group with the center hole diameter of Φ10 mm has the highest peak stress of 147.00 MPa, and the specimen group with the center hole diameter of Φ8 mm has a medium peak stress of 143.70 MPa.

As is illustrated in Figure 9, the average effective elastic modulus (obtained by averaging the elastic modulus of each granite specimen group measured through the uniaxial compression experiment) of the rock specimen decreases initially and increases gradually with the increase of center hole diameter, but the average effective elastic modulus of the three groups with a center hole is lower than that of the last group with no center hole because the strain increases while the bearing capacity decreases under the operation of servo press after the rock specimen with a center hole has undergone internal damage. As the rock specimen with the center hole diameter of Φ6 mm suffers the most severe internal damage, its effective elastic modulus is the lowest.

Figure 10 reveals the distribution of average peak stress (obtained by averaging the peak stress of each granite specimen group measured through the uniaxial compression experiment) of the four specimen groups, among which the specimen group with the center hole diameter of Φ6 mm has the lowest peak stress and the peak stress of the specimen group with the center hole diameter of Φ10 mm is higher than that of the specimen group with the center hole diameter of Φ8 mm. In case of constant power of an electric hammer, the impact load of it is constant. According to formula (2), the relation of radial stress of the center hole wall and drill bit diameter can be reflected in Figure 11:

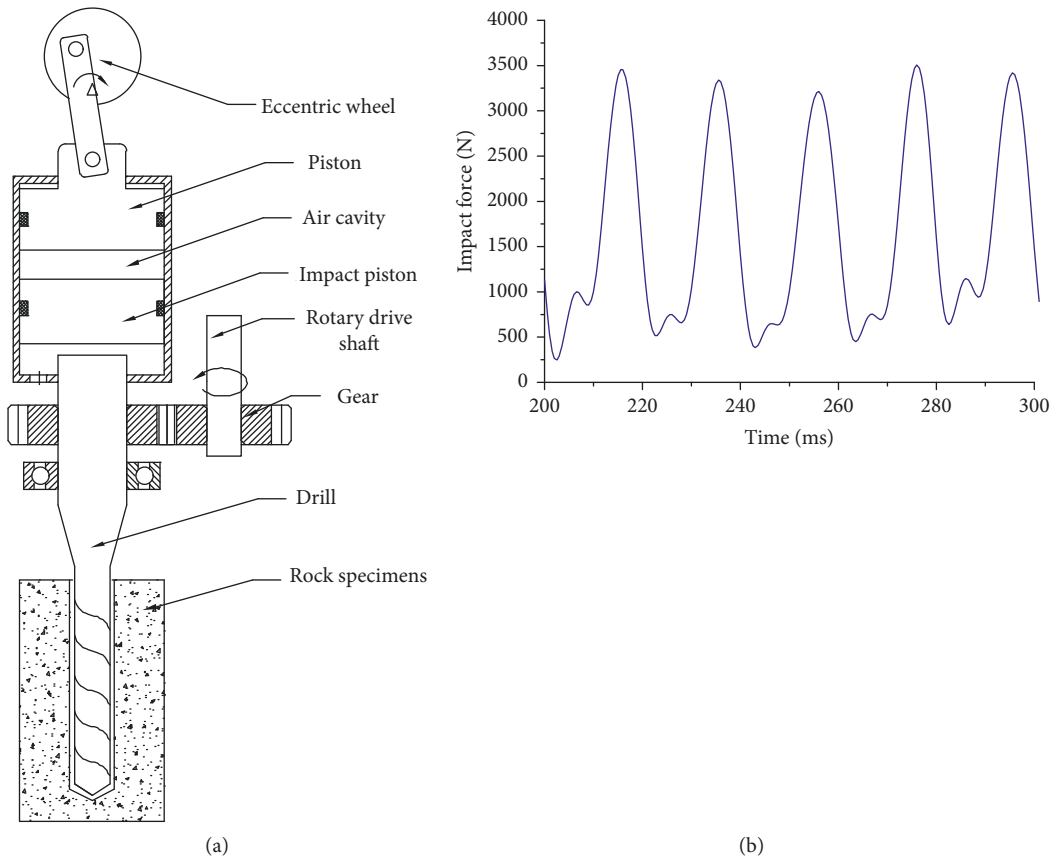

Figure 5: Principle of electric hammer's drilling and implementation. (a) Schematic diagram of electric hammer's drilling. (b) Waveform of electric hammer's impact force.

Figure 6: Processed rock specimens.

compared with the drill bit of Φ8 mm and Φ10 mm, the drill bit of Φ6 mm creates a higher radial stress, causing the most serious damage to the surrounding rock around the center hole wall. Therefore, to drill a bigger center hole that causes greater damage to the surrounding rock around the center hole wall, the impact load P_m should be increased.

4.5. Comparison between the Experimental and Theoretical Constitutive Relations of Rock under High-Frequency Impact Load. On the basis of the damage constitutive model in formula (18), the fitting parameters of the constitutive model of each group are made clear by the analysis of experimental data, which are shown in Table 3. The parametric cohesion C, angle of internal friction ϕ, and viscosity coefficient η are measured by the MTS 815 rock mechanics testing system.

As is shown in Figure 12, the experimental curve is in accordance with the theoretical curve, demonstrating the rationality of the damage model that effectively reflects the relations between rock strength and high-frequency impact load. However, there is a certain deviation on the slope of the initial stage between the theoretical curve and experimental curve, which fails to reflect the elastic modulus of rock specimens in the initial stage under impact load. Meanwhile, the model also fails to reflect some fluctuations in the experimental curve, especially the fluctuation surrounding the peak stress. The deviation may originate from the selection of model parameters or the imperfection of the damage model itself, both of which need further improvement.

Table 1: Physical and mechanical parameters of granite.

Type of rock	Density (g/cm^3)	Uniaxial compressive strength (MPa)	Elastic modulus (GPa)	Poisson's ratio	Cohesion (MPa)	Angle of internal friction (degrees)
Granite	2.68	150.78	35.06	0.26	28.48	48.497

(a) (b)

Figure 7: INSTRON 1346 universal material testing machine and diagrammatic sketch of the experimental system.

Table 2: Physical parameters of granite specimens.

Specimen number	Length (mm)	External diameter (mm)	Center hole diameter (mm)	Mass (g)
1-1	99.98	49.04	Null	506.8
1-2	100.14	49.06	Null	507.1
1-3	100.04	49.10	Null	506.6
1-4	100.16	48.80	Null	507.2
1-5	100.18	48.74	Null	507.5
2-1	100.16	49.2	6.24	501.1
2-2	98.68	49.20	6.24	493.7
2-3	100.36	48.64	6.26	490.1
2-4	99.68	49.20	6.26	499.1
2-5	98.08	49.16	6.28	489.1
3-1	99.74	49.18	8.14	490.6
3-2	97.88	49.20	8.08	489.1
3-3	99.68	49.22	8.10	494.0
3-4	98.90	49.20	8.12	489.0
3-5	100.56	49.20	8.08	496.6
4-1	100.10	49.20	10.36	485.8
4-2	100.60	49.20	10.40	487.6
4-3	100.44	49.22	10.46	486.7
4-4	100.50	49.20	10.50	487.1
4-5	100.64	49.20	10.42	485.1

4.6. Damage Properties of Surrounding Rock under High-Frequency Impact Load. Through the deduction process of surrounding rock damage D_0, it can be implied that D_0 is a function associated with impact load P_m, center hole diameter a, and center hole radius in the plastic zone r_1. As is demonstrated in Figure 5, the impact force of the electric hammer is nearly constant, so D_0 and r_1 are a function of a. The ratio of r_1 to a is defined as the damage ratio denoted by β. In Figure 13, under certain frequency and certain amount of impact load, the surrounding rock

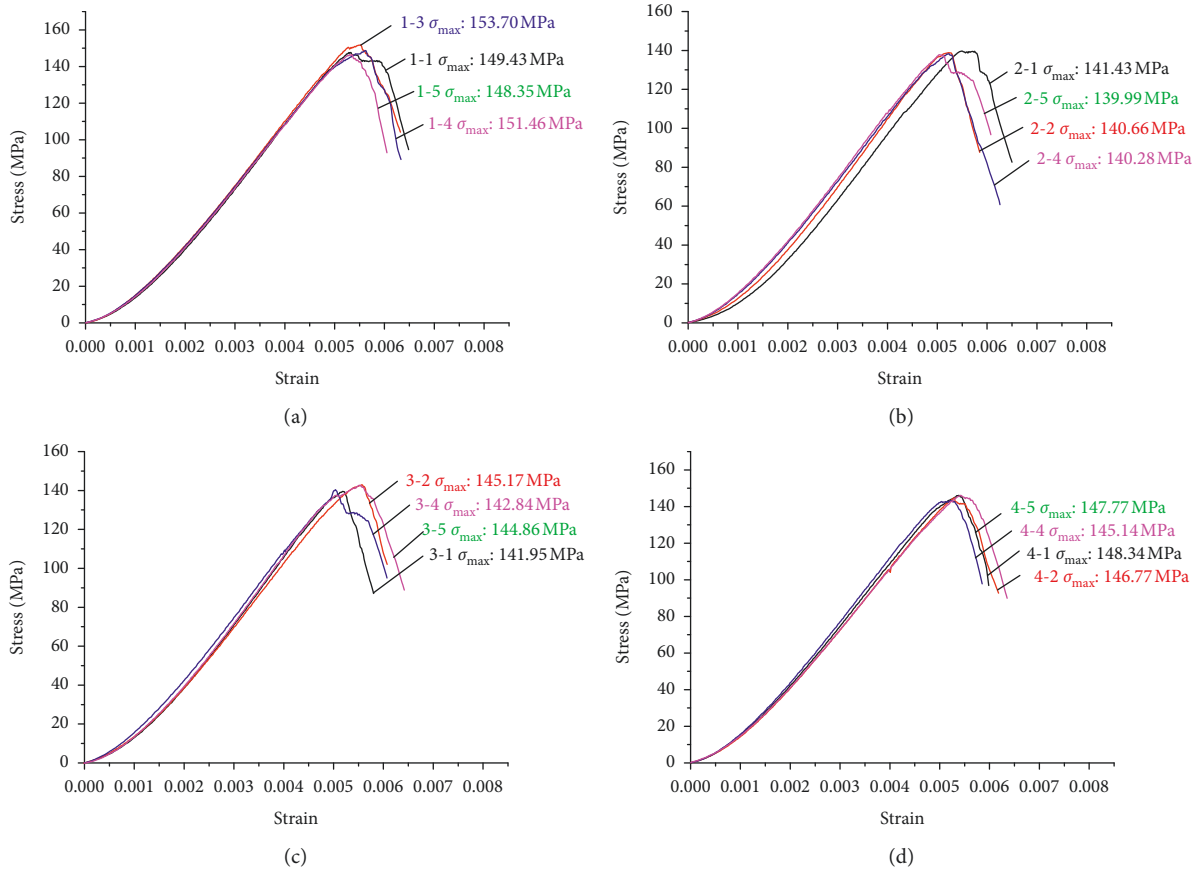

Figure 8: Stress-stain curves of granite specimen groups. (a) The first specimen group. (b) The second specimen group. (c) The third specimen group. (d) The fourth specimen group.

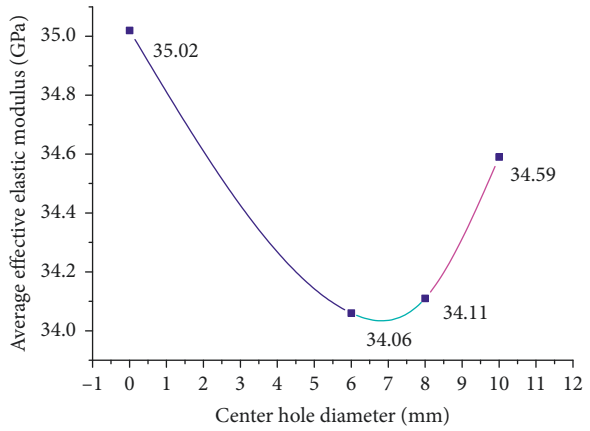

Figure 9: Average effective elastic modulus of each specimen group.

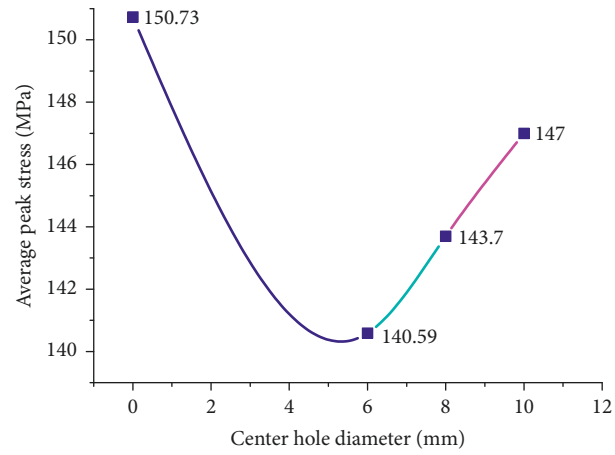

Figure 10: Average peak stress distribution of each specimen group.

damage D_0 and damage ratio β tend to decrease with the increase of center hole diameter r_0. This coincides with the energy dissipation law. As the energy consumed in drilling a larger center hole is more than that consumed in drilling a smaller one, the radius of rock damage surrounding a larger center hole is smaller than that surrounding a smaller one. Therefore, as is illustrated in Figure 1, to drill a center hole with a larger reaming diameter, impact load and center hole radius should be taken into consideration.

5. Conclusion

In this study, the theoretical model of surrounding rock damage under impact load is established according to

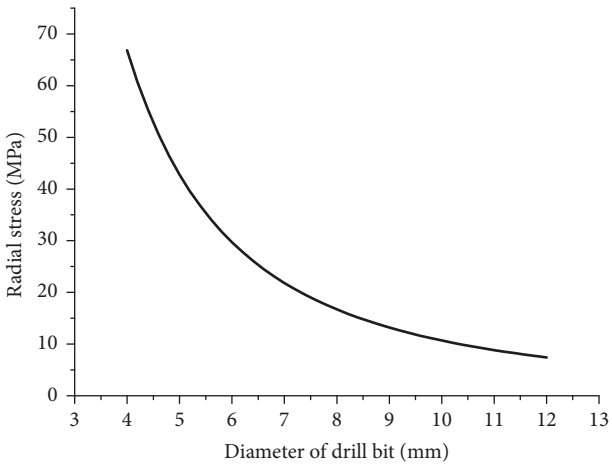

Figure 11: Relation curve between radial stress and drill bit diameter.

Table 3: Experimental parameters and fitting parameters.

Specimen number	Parameters						
	E (GPa)	ϕ (°)	μ	C (MPa)	m	F_0	η
1-1	35.33	48.5	0.26	28.48	4.22	206.5	0.2
2-1	33.74	48.5	0.26	28.48	13.58	149.54	0.2
3-1	34.49	48.5	0.26	28.48	19.90	143.29	0.2
4-1	34.63	48.5	0.26	28.48	22.46	141.59	0.2

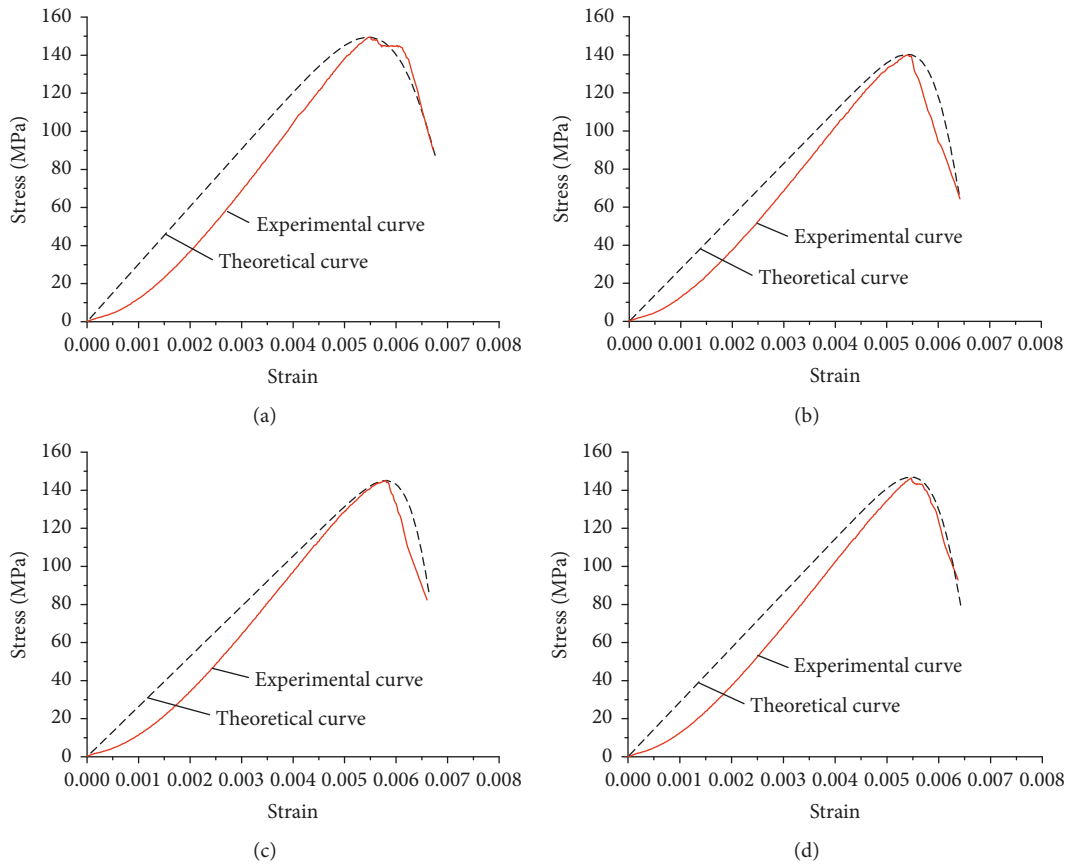

Figure 12: Contrast diagram between the theoretical and experimental curves of granite specimen groups. (a) Specimen group 1-1. (b) Specimen group 2-4. (c) Specimen group 3-2. (d) Specimen group 4-2.

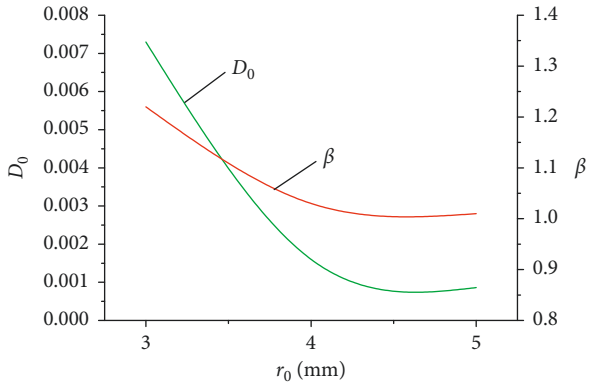

Figure 13: Surrounding rock damage of granite specimen groups and variation of ratio with the center hole radius.

Mohr–Coulomb's strength theory, and the damage constitutive model of rock under impact load is deduced with the aid of the statistical damage constitutive model based on the Weibull distribution. By drilling the center hole of standard granite specimens under impact load and applying them to the uniaxial compression experiments by using the INSTRON 1346 universal material testing machine, the experimental results show the peak stress of rock specimens with a center hole is lower than that of rock specimens with no center hole, indicating that impact stress has caused certain damage to the surrounding rock. Besides, the peak stress of rock specimens with the smallest center hole diameter is the lowest among the three specimen groups shown in the stress-strain curve, which suggests the rock surrounding a smaller center hole diameter suffers more serious damage than that surrounding a larger one.

After drilling the center hole under impact load, the surrounding rock damage D_0 and damage ratio β show a decreasing trend with the increase of center hole diameter in accordance with the energy dissipation laws. As drilling a larger center hole consumes more energy than drilling a smaller one, the damage ratio of rock surrounding a larger center hole is smaller than that surrounding a smaller one.

Data Availability

The experimental data used to support the findings of this study are included within the article.

Conflicts of Interest

The authors declare that there are no conflicts of interest regarding the publication of this paper.

Acknowledgments

The research presented in this paper was supported by the National Natural Science Foundation of China (Grant no. 51774340).

References

[1] L. X. Huang and Y. B. Chen, "Rock dynamics in China: past, present and future," *Chinese Journal of Rock Mechanics and Engineering*, vol. 22, no. 11, pp. 1881–1886, 2003.

[2] J. Z. Liu, J. Y. Xu, X. C. Lü, Z. D. Wang, and L. Zhang, "Study on dynamic behavior and damage constitutive model of rock under impact loading with confining pressure," *Engineering Mechanics*, vol. 21, no. 02, pp. 55–63, 2012.

[3] J. Y. Xu, X. C. Lü, J. Zhang et al., "Research on energy properties of rock cyclical impact damage under confining pressure," *Chinese Journal of Rock Mechanics and Engineering*, vol. 29, no. 2, pp. 4159–4165, 2010.

[4] X. B. Li, Y. J. Zuo, and C. D. Ma, "Constitutive model of rock under coupled static-dynamic loading with intermediate strain rate," *Chinese Journal of Rock Mechanics and Engineering*, vol. 25, no. 5, pp. 865–874, 2006.

[5] C. Cai, K. S. Wu, X. H. Yuan, and S. J. Cheng, "Damage constitutive model of rock under medium and low strain rates," *Rock and Soil Mechanics*, vol. 36, no. 3, pp. 795–802, 2015.

[6] Z. T. Lu and Z. L. Wang, "Triaxial tests on dynamic properties of granite under intermediate and high strain rates," *Chinese Journal of Geotechnical Engineering*, vol. 38, no. 6, pp. 1087–1094, 2016.

[7] C. Wang and L. Z. Tang, "Constitutive model of rock under one dimensional high stress and repeated impact loading," *Chinese Journal of Rock Mechanics and Engineering*, vol. 34, no. 1, pp. 2868–2878, 2015.

[8] X. B. Li and D. S. Gu, *Rock Impact Dynamics*, Central South University of Technology Press, Changsha, China, 1994.

[9] X. B. Li, Z. L. Zhou, Z. Y. Ye et al., "Study of rock mechanical characteristics under coupled static and dynamic loads," *Chinese Journal of Rock Mechanics and Engineering*, vol. 27, no. 7, pp. 1387–1395, 2008.

[10] X. Li, Z. Zhou, T.-S. Lok, L. Hong, and T. Yin, "Innovative testing technique of rock subjected to coupled static and dynamic loads," *International Journal of Rock Mechanics and Mining Sciences*, vol. 45, no. 5, pp. 739–748, 2008.

[11] J. J. Zhu, X. B. Li, F. Q. Gong, and S. M. Wang, "Dynamic characteristics and damage model for rock under uniaxial cyclic impact compressive loads," *Chinese Journal of Geotechnical Engineering*, vol. 35, no. 3, pp. 531–539, 2013.

[12] F. Q. Gong, X. B. Li, X. L. Liu et al., "Experimental study of dynamic characteristics of sandstone under one-dimensional coupled static and dynamic loads," *Chinese Journal of Rock Mechanics and Engineering*, vol. 29, no. 10, pp. 2076–2085, 2010.

[13] X. F. Li, H. B. Li, K. Liu et al., "Research on the dynamic properties and fracture characteristics of rocks subject to impact loading," *Chinese Journal of Rock Mechanics and Engineering*, vol. 36, no. x, pp. 1–12, 2017.

[14] C. Zou, L. N. Y. Wong, J. J. Loo, and B. S. Gan, "Different mechanical and cracking behaviors of single-flawed brittle gypsum specimens under dynamic and quasi-static loadings," *Engineering Geology*, vol. 201, pp. 71–84, 2016.

[15] M. Tao, A. Ma, W. Cao, X. Li, and F. Gong, "Dynamic response of pre-stressed rock with a circular cavity subject to transient loading," *International Journal of Rock Mechanics and Mining Sciences*, vol. 99, pp. 1–8, 2017.

[16] H. B. Li, X. Xia, J. C. Li et al., "Rock damage control in bedrock blasting excavation for a nuclear power plant," *International Journal of Rock Mechanics and Mining Sciences*, vol. 48, no. 2, pp. 210–218, 2011.

[17] M. Ramulu, A. K. Chakraborty, and T. G. Sitharam, "Damage assessment of basaltic rock mass due to repeated blasting in a railway tunnelling project—a case study," *Tunnelling and Underground Space Technology*, vol. 24, no. 2, pp. 208–221, 2009.

[18] M. G. Liu, G. H. Zhang, S. B. Liu et al., "Research on accumulative damage effect of interlaid rock in Damaoshan tunnel group with small clear distance," *Chinese Journal of Rock Mechanics and Engineering*, vol. 28, no. 7, pp. 1363–1369, 2009.

[19] J. F. Jin, X. B. Li, G. S. Wang et al., "Failure modes and mechanisms of sandstone under cyclic impact loadings," *Journal of Central South University: Science and Technology*, vol. 43, no. 4, pp. 1453–1461, 2012.

[20] J. F. Jin, X. B. Li, Z. Q. Yin et al., "A method for defining rock damage variable by wave impedance under cyclic impact loadings," *Rock and Soil Mechanics*, vol. 32, no. 5, pp. 1385–1393, 2011.

[21] J. F. JinX. B. Li et al., "Evolution model for damage accumulation of rock under cyclic impact loadings and effect of static loads on damage evolution," *Chinese Journal of Rock Mechanics and Engineering*, vol. 33, no. 8, pp. 1662–1671, 2014.

[22] D. N. Lin and S. R. Chen, "Experimental study on damage evolution law of rock under cyclical impact loadings," *Chinese Journal of Rock Mechanics and Engineering*, vol. 24, no. 22, pp. 4094–4098, 2005.

[23] J. B. Martino and N. A. Chandler, "Excavation-induced damage studies at the underground research laboratory," *International Journal of Rock Mechanics and Mining Sciences*, vol. 41, no. 8, pp. 1413–1426, 2004.

[24] I. L. Meglis, T. Chow, C. D. Martin, and R. P. Young, "Assessing in situ microcrack damage using ultrasonic velocity tomography," *International Journal of Rock Mechanics and Mining Sciences*, vol. 42, no. 1, pp. 25–34, 2005.

[25] L. Weng, Z. Wu, and X. Li, "Mesodamage characteristics of rock with a pre-cut opening under combined static-dynamic loads: a nuclear magnetic resonance (NMR) investigation," *Rock Mechanics and Rock Engineering*, vol. 51, no. 8, pp. 2339–2354, 2018.

[26] N. Jiang, C. B. Zhou, X. Luo, and S. Lu, "Damage characteristics of surrounding rock subjected to vcr mining blasting shock," *Shock and Vibration*, vol. 2018, Article ID 373021, 8 pages, 2015.

[27] J. Yang, W. Lu, Y. Hu, M. Chen, and P. Yan, "Numerical simulation of rock mass damage evolution during deep-buried tunnel excavation by drill and blast," *Rock Mechanics and Rock Engineering*, vol. 48, no. 5, pp. 2045–2048, 2015.

[28] A. Golshani, M. Oda, Y. Okui, T. Takemura, and E. Munkhtogoo, "Numerical simulation of the excavation damaged zone around an opening in brittle rock," *International Journal of Rock Mechanics and Mining Sciences*, vol. 44, no. 6, pp. 835–845, 2007.

[29] X.-D. Zhao, H.-X. Zhang, and W.-C. Zhu, "Fracture evolution around pre-existing cylindrical cavities in brittle rocks under uniaxial compression," *Transactions of Nonferrous Metals Society of China*, vol. 24, no. 3, pp. 806–815, 2014.

[30] S. Y. Wang, S. W. Sloan, D. C. Sheng, and C. A. Tang, "Numerical analysis of the failure process around a circular opening in rock," *Computers and Geotechnics*, vol. 39, pp. 8–16, 2012.

[31] W. C. Wang, L. M. Dou, J. Li, K. Kang, and L. Feng, "Numerical Investigation of Damage Risks of Roadway Surrounding Rocks under Oblique Incident Dynamic Loads," *Shock and Vibration*, vol. 2017, Article ID 6298372, 13 pages, 2017.

[32] X. C. Lü, J. Y. Xu, H. H. Ge et al., "Effects of confining pressure on mechanical behaviors of sandstone under dynamic impact loads," *Chinese Journal of Rock Mechanics and Engineering*, vol. 29, no. 1, pp. 193–201, 2010.